

Targeted alteration of real and imaginary refractive index of biological cells by histological staining

L. Cherkezyan,¹ H. Subramanian,¹ V. Stoyneva,¹ J. D. Rogers,¹ S. Yang,¹
D. Damania,¹ A. Taflove,² and V. Backman^{1,*}

¹Biomedical Engineering Department, Northwestern University, Evanston, Illinois 60208, USA

²Electrical Engineering and Computer Science Department, Northwestern University, Evanston, Illinois 60208, USA

*Corresponding author: v-backman@northwestern.edu

Received December 2, 2011; revised January 27, 2012; accepted February 11, 2012;
posted February 13, 2012 (Doc. ID 159305); published May 9, 2012

Various staining techniques are commonly used in biomedical research to investigate cellular morphology. By inducing absorption of light, staining dyes change the intracellular refractive index due to the Kramers–Kronig relationship. We present a method for creating 2D maps of real and imaginary refractive indices of stained biological cells using their thickness and absorbance. We validate our technique on dyed polystyrene microspheres and quantify the alteration in refractive index of stained biological cells. We reveal that specific staining of individual organelles can increase their scattering cross-section by orders of magnitudes, implying a major impact in the field of biophotonics. © 2012 Optical Society of America

OCIS codes: 160.4760, 170.1530, 170.0180, 300.6550, 290.0290.

Staining provides a tool for visualization of macromolecules, biological cells, and tissues in applications that extend from basic biology to clinical diagnostics [1,2]. Within the field of optics, the change in light scattering properties of stained organelles caused by the absorption of specific dyes is used to determine their refractive indices [3]. However, while most of the attention has been focused on the absorption (i.e., the imaginary part of the refractive index) introduced by staining dyes, the subsequent alteration in the real part of the refractive index according to the Kramers–Kronig relation has often been overlooked [4,5]. A recently proposed linear relationship between the real and imaginary parts of refractive index does not treat the effects of spectral dispersion in either quantity [6]. In this Letter, we demonstrate a method to quantify the wavelength-dependent change in both the real and imaginary parts of the refractive index of epithelial cells caused by histological stains such as hematoxylin and eosin-containing cytochrome.

We construct 2D maps for real and imaginary refractive indices (n' and n'') of stained cells as a function of wavelength λ as follows: first, we calculate the n'' after measuring the transmission intensity I and the sample thickness L using

$$I(x, y, \lambda) = I_0(x, y, \lambda_0) \exp \left\{ - (4\pi/\lambda) \int_0^{L(x,y)} n''(x, y, z, \lambda) dz \right\}, \quad (1)$$

where $I_0(x, y, \lambda_0)$ is the transmission intensity at a wavelength λ_0 where absorption is absent (to isolate n'' from other causes of attenuation). For dyes used in this study $\lambda_0 = 700$ nm. Then, we extract the $n'(\lambda)$:

$$n'' = \chi''_{\text{dye}}/2n', \quad n' = n_0 \sqrt{1 + (\chi'_{\text{dye}} + n''^2)/n_0^2}, \quad (2)$$

where $\chi'_{\text{dye}} + j\chi''_{\text{dye}}$ is the electric susceptibility of dye molecules embedded in a nonabsorbing material with a refractive index n_0 . χ'_{dye} is determined from χ''_{dye} using Kramers–Kronig relations [4,5,7]

$$\chi'_{\text{dye}}(k) = (2/\pi)P \int_0^\infty k' \chi''_{\text{dye}}(k') / ((k'^2 - k^2) dk'),$$

$$\chi''_{\text{dye}}(k) = - (2k/\pi)P \int_0^\infty \chi'_{\text{dye}}(k') / (k'^2 - k^2) dk', \quad (3)$$

where P denotes Cauchy principal value and k is the wavenumber $k = 2\pi/\lambda$. Our instrumentation includes an atomic force microscope (AFM, Bruker Bioscope II) with 39 nm resolution to measure the thickness $L(x, y)$ and a custom-built spectroscopic microscope (SM) to image the sample, as well as measure the wavelength-dependent transmission through it $I(x, y, \lambda)$. The sample of interest is mounted between 2 glass slides using Permaslip (Alban Scientific) to remove specular reflections at the specimen-air interface. The bottom glass slide is coated with a 100 nm layer of Aluminum (Deposition Research Lab) in order to redirect the transmitted light back through the sample onto the detector (Fig. 1). Thus, the recorded signal (normalized by the reflectance of a mirror) represents transmission after a double pass through the sample, which effectively increases its thickness and therefore the signal-to-noise ratio of absorption measurements.

In order to establish this SM-based technique as a method for recovering refractive index change after

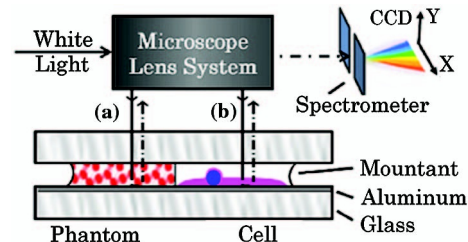


Fig. 1. Schematic of the SM and sample design: reflected-light Kohler illumination brightfield microscope (60× objective lens; N.A. 0.4) projects sample image through a grating spectrometer on a CCD camera. A stage under the spectrometer spatially scans the sample image. (a) dyed microspheres phantom; (b) stained biological cell.

staining, we first tested a controlled phantom. The phantom consisted of dry red-dyed polystyrene microspheres suspended in a droplet of Permaslip between 2 glass slides (Polybead, diameter $a = .2 \mu\text{m}$) as illustrated in Fig. 1(a). To account for the difference between the dye distribution within this phantom and within a stained cell, we transformed Eq. (1) into an analogous expression for a suspension of spheres with absorption efficiency $Q_{\text{abs}}(\lambda)$ and total number per voxel $N(x, y)$: $I(x, y, \lambda) = I_0 \exp(-N(x, y)\pi(a/2)^2 Q_{\text{abs}}(\lambda))$. Thus, after the transmission spectrum was acquired by SM, the $Q_{\text{abs}}(\lambda)$ was obtained. This determined both parts of the dyed sphere complex refractive index ($n(\lambda)$): the $n''(\lambda)$ was reconstructed from [8]

$$\text{Im} \left\{ \frac{n^2(\lambda) - n_{\text{med}}^2(\lambda)}{n^2(\lambda) + 2n_{\text{med}}^2(\lambda)} \right\} = -\frac{\lambda}{8\pi a} Q_{\text{abs}}(\lambda), \quad (4)$$

where Im denotes the imaginary part of a complex variable, and “med” refers to the surrounding medium; the $n'(\lambda)$ was obtained from Eq. (2), with n_0 corresponding to unstained (white) polystyrene. Note that unlike the $n(x, y, \lambda)$ of a biological cell, the n of a polystyrene sphere is independent of location (x, y) .

To verify the reliability of extracted $n'(\lambda)$ and $n''(\lambda)$ of dyed spheres we quantified them independently with the integrating sphere (IS) technique. As the IS required a large homogeneous sample, the spheres were suspended in water instead of the rapidly solidifying Permaslip. After the transmittance and reflectance were measured with IS, the absorption and reduced scattering coefficients were recovered by inverse adding-doubling (IAD) [9–11] algorithm and normalized by known sphere concentration. Eq. (4) was then used to calculate n'' . The $n''(\lambda)$ and the reduced scattering cross-section σ'_{sca} of dyed microspheres obtained by both SM and IS-IAD are shown in Fig. 2. Spectral profiles of n'' show good agreement within one standard error of each other with a 7 nm peak shift noticeable from 555 to 575 nm [Fig. 2(a)]. This can be attributed to the chemical interactions of the dye with different solvents (water and Permaslip). Since n' alone cannot be calculated using IS-IAD, we instead compared the σ'_{sca} as it is defined by both n' and n'' . The corresponding σ'_{sca} for the SM was recovered using Mie theory [12]. A perfect match between the σ'_{sca} obtained by both IS-IAD and SM is seen in Fig. 2(b). These results confirmed the reliability of our technique in measuring the complex refractive index of dyed materials.

Next, we quantified the complex refractive index of stained squamous epithelial cells extracted from

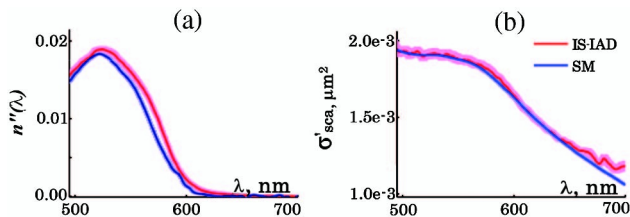


Fig. 2. (a) n'' of dyed polystyrene microspheres and (b) their reduced scattering cross-section. IS-IAD data appears in red and is based on post-processing of the SM measurements in blue. Standard errors in corresponding shaded colors.

buccal mucosa. The cells were smeared onto the metallic surface of coated slides using a cytobrush (CooperSurgical) fixed with 95% ethanol and stained with conventional nuclear and cytoplasmic dyes: hematoxylin (H) (absorption peak at 628 nm) and Cytostain (absorption peak of eosin (E) at 536 nm) (Richard-Allan, Thermo Scientific). Cell thickness was obtained using AFM, after which a glass slide was mounted on top of the sample as described above. To calculate n' and n'' of a stained cell using Eq. (2), the refractive index of an unstained cell (n_0) is required. Although the reported refractive index of dehydrated cells is between 1.50 and 1.55 [13,14], the exact values are poorly investigated. In this study we evaluated n_0 using Gladstone–Dale relation $n = n_w + \alpha\rho$, where n_w is the refractive index of water, α is the specific refractive increment (0.18 ml/g), and ρ is the cell dry density which was approximated as that of stratum mucosum (1.15 g/ml) [15]. This resulted in the average $n_0(\lambda)$ of 1.54 [Fig. 3(b)].

As a demonstration, we subsequently evaluated $n'(\lambda)$ and $n''(\lambda)$ of three squamous epithelial cells. The absorption strength varied greatly between them and the average peak values of the measured $n''(\lambda)$ were 0.05, 0.06, and 0.08. In response, according to Kramers–Kronig relations [Eq. (3)], the $n'(\lambda)$ decreased at λ shorter than the absorption peak and increased at λ longer than the absorption peak by 0.06, 0.08, and 0.11 respectively. Thus, we revealed that the change in the intracellular refractive index induced by staining is significantly greater than the reported endogenous spatial variations of it (0.02, [16]).

The summary of results from a typical cell is illustrated in Fig. 3. Note that the refractive index maps represent vertically averaged values and thus inherently underestimate its spatial variations. For instance, consider the voxel circled in red that includes nucleus surrounded by cytoplasm layers from above and below. The spectrum of $n''(\lambda)$ corresponding to it has peaks at the absorption wavelengths of both H and E. Its magnitude at 536 nm suggests a lower effect of E in that region compared to the purely cytoplasmic voxels (blue and orange). However, this is a sheer consequence of averaging throughout the volume where E is not distributed homogeneously. Similarly, since the affinity of dye molecules is determined by their chemical properties, it is not uniformly spread within a biological cell. As a result, the refractive index change at the site of their localization is larger than when averaged throughout the cell thickness.

Of particular importance is that, by changing the spatial distribution of refractive index, staining significantly affects the extinction properties of intracellular compartments. As an illustration, using the Mie theory [12], we calculated the absorption and scattering efficiencies of spheres with refractive indices before and after staining corresponding to the black and orange spectra in Fig. 3(b). As seen in Fig. 3(d), while the staining-induced absorption efficiency increases with particle size, in contrast the amplification of the scattering efficiency decreases. Moreover, for intracellular particles such that $ka(n_{\text{particle}}/n_{\text{med}} - 1) \ll 1$, introduction of n'' can amplify their scattering cross-sections by orders of magnitudes [17]. Interestingly, with the increase of sphere diameter, the spectral profile of the scattering amplification gradually changes from

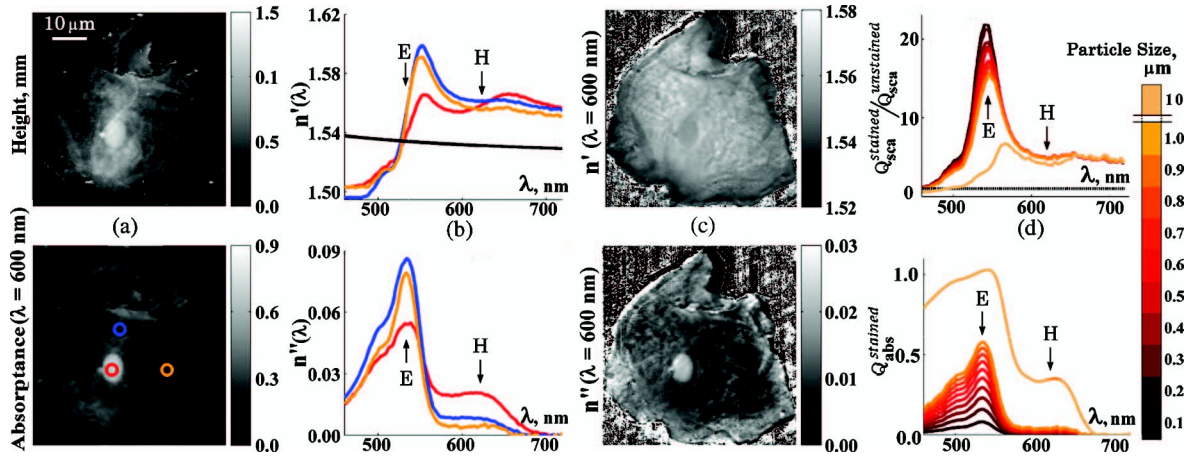


Fig. 3. (a) shows the measured cell height and absorbance at 600 nm. (b) illustrates the n' and n'' for 3 areas (black corresponds to unstained); letters H and E point to the absorption peaks of hematoxylin and eosin correspondingly. (c) illustrates the spatial distribution of n' and n'' at 600 nm within the cell. (d) Size-dependent absorption efficiency (Q_{abs}) and amplification of scattering efficiency (Q_{sca}) (refractive index of surrounding medium assumed to be 1.52).

resembling the spectral shape of $n''(\lambda)$ into resembling that of the $n'(\lambda)$ as also was predicted in [8].

In conclusion, while the absorption of staining dyes is used in routine microscopy, its imaging resolution is diffraction limited. Meanwhile, the refractive index change demonstrated here suggests an alternative use of dyes as contrast agents in the field of light scattering to investigate subdiffractional structures such as specific organelles, chromatin fibers, proteins, etc. In clinic, this effect can advance cancer diagnosis when utilized by scattering-based techniques such as optical coherence microscopy (OCM), light scattering spectroscopy (LSS), confocal light absorption and scattering spectroscopy (CLASS), and partial wave spectroscopic (PWS) microscopy [18,19].

This work was supported by National Institutes of Health (NIH) grants R01CA128641, R01EB003682, and R01CA155284, and National Science Foundation (NSF) grant CBET-0937987.

References

1. E. D. P. De Robertis, F. A. Saez, and E. M. F. De Robertis, *Cell Biology*, 6th ed. (Saunders, 1975).
2. E. S. Cibas and B. S. Ducatman, *Cytology: Diagnostic Principles and Clinical Correlates* (Saunders, 1996).
3. J. D. Wilson, W. J. Cottrell, and T. H. Foster, *J. Biomed. Opt.* **12**, 014010 (2007).
4. R. d. L. Kronig, *J. Opt. Soc. Am.* **12**, 547 (1926).
5. H. A. Kramers, *Atti del Congresso Internazionale dei Fisici* **2**, 545 (1927).
6. S. Uttam, R. K. Bista, D. J. Hartman, R. E. Brand, and Y. Liu, *J. Biomed. Opt.* **16**, 116013 (2011).
7. V. Lucarini, *Kramers-Kronig Relations in Optical Materials Research* (Springer, 2005).
8. H. C. v. d. Hulst, *Light Scattering by Small Particles* (Wiley, 1957).
9. S. A. Prahl, "Inverse adding-doubling software," <http://omlc.org/software/iad/index.html>.
10. J. W. Pickering, S. A. Prahl, N. Vanwieringen, J. F. Beek, H. J. C. M. Sterenborg, and M. J. C. Vangemert, *Appl. Opt.* **32**, 399 (1993).
11. S. A. Prahl, M. J. C. Vangemert, and A. J. Welch, *Appl. Opt.* **32**, 559 (1993).
12. C. Maetzler, "MATLAB functions for Mie scattering and absorption," Research Report 2002-08 (Bern, 2002).
13. D. J. Cook, in *Cellular Pathology*, 2nd ed. (Scion, 2006), pp. 67–104.
14. G. C. Crossmon, *Stain Technol.* **24**, 241 (1949).
15. H. G. Davies, M. H. F. Wilkins, J. Chayen, and L. F. Lacour, *Q. J. Microsc. Sci.* **95**, 271 (1954).
16. J. M. Schmitt and G. Kumar, *Appl. Opt.* **37**, 2788 (1998).
17. G. W. Kattawar and G. N. Plass, *Appl. Opt.* **6**, 1377 (1967).
18. N. N. Boustany, S. A. Boppart, and V. Backman, *Annu. Rev. Biomed. Eng.* **12**, 285 (2010).
19. H. Subramanian, P. Pradhan, Y. Liu, I. R. Capoglu, J. D. Rogers, H. K. Roy, R. E. Brand, and V. Backman, *Opt. Lett.* **34**, 518 (2009).